An Algorithm for Real-Time Rainfall Rate Estimation by Using Polarimetric Radar: RIME

FRANCESCO SILVESTRO AND NICOLA REBORA

CIMA Research Foundation, Savona, Italy

LUCA FERRARIS

CIMA Research Foundation, Savona, and DIST, University of Genova, Genova, Italy

(Manuscript received 11 February 2008, in final form 22 July 2008)

ABSTRACT

Polarimetric radars provide measurements that describe the shape and dimensions of hydrometeors and are unaffected by calibration, attenuation, and the presence of ice. These measurements can potentially lead to a more detailed description of hydrometeors and to an improvement in quantitative rainfall rate estimation. The authors present an algorithm that exploits polarimetric measures for rain-rate estimation and investigate its application in a real-time framework by using measurements from the C-band polarimetric radar at Monte Settepani in Savona, Italy. It is based on a flowchart decision tree that allows the use of the best rain-rate retrieval algorithm, depending on the value of polarimetric variables. The methodology was applied to a real-time framework for more than a year, and the results were presented for all the significant events observed during the test period. To evaluate the performance of the algorithm, a comparison was made with rain gauge observation from a dense regional network. The performances of the algorithm were compared with those obtained by standard operational *Z–R* formulations to evaluate the benefit of this approach for operational applications.

1. Introduction

Quantitative precipitation estimation is a crucial issue for operational radar applied to hydrological prediction and modeling. In the last two decades, the benefits of using polarimetric radar have been shown, and polarimetry has proved to be a crucial element for data quality, attenuation correction, and improvement of rain-rate estimation (Bringi and Chandrasekar 2001; Meischner 2004). Many techniques for rain-rate estimation involving polarimetric variables have been proposed and tested (e.g., Ryzhkov and Zrnic 1996; Ryzhkov et al. 2005), however, an analysis of polarimetric measurements applied to real-time rain-rate estimation is still lacking—for C-band radar systems, in particular.

In this work we present some analysis on the C-band version of an existing methodology proposed by Cifelli et al. (2003) for S-band that has been simplified to comply with operational requirements. Then we applied it to an operational radar with operational scan strategies. The task is to analyze if a relatively simple algorithm, which involves polarimetric variables for estimating rain rate, can perform well in a real-time framework. The main objective of this work was to investigate the possible improvements to operational polarimetric rainfall estimation and to make a comparison with the use of traditional *Z–R* techniques. In addition, this work has enabled polarimetric capabilities to be tested on a C-band operational system. From September 2005 to October 2007, nine events were selected as test cases; the polarimetric algorithm was also tested for a continuous period of about six months to evaluate its possible application in an operational framework.

In evaluating the capability of radar as a tool for the quantitative estimation of precipitation, it is a common approach to compare radar measurements of rainfall with those given by one or more rain gauges. The subject was fully investigated and discussed (Zawadzki 1975; Jayakrishnan et al. 2004), and different comparison methodologies were implemented.

Corresponding author address: Francesco Silvestro, CIMA Research Foundation, Via Magliotto 2, Savona 17100, Italy.
E-mail: francesco.silvestro@cimafoundation.org

DOI: 10.1175/2008JHM1015.1

TABLE 1. Characteristics of Settepani C-band radar system (S/N = signal to noise ratio).

Radar characteristics	
Radar model	GPM250C (Selex-Gematronik)
Radar height	1400 m
Beam width	1°
Operational frequency	5600–5650 MHz
Sensitivity	−10 dBZ, with S/N = 0 dB at 50 km
Pulse lengths	0.5/ 1.5/ 3.0 μs
Peak power	≥250 kW
Transmitter	coherent, klystron

TABLE 2. Operational polarimetric scan characteristics.

Radar characteristics	
PRF	1100 Hz
Max distance	136 km
Beam width	1°
Pulse length	0.5 μs
Bin radial resolution	0.3 km
Number of elevations	11
Scan time	10 min
Measured moments	Z_H, Z_{DR}, V_r, ϕ_{DP}, ϱ_{HV}(Lag 1)

Here, we have adopted a method of comparison that tries to overcome the problems caused by different characteristics of measurements. This method avoids both the adoption of rain gauge interpolation techniques and the use of areal means that can cause smoothing problems. It also takes into consideration the inhomogeneity of coverage of the operational rain gauge network used.

The paper is organized as follows: section 2 describes the two operational systems of measurement: (i) radar system and (ii) rain gauge network. Section 3 describes the algorithms used, and section 4 describes how these algorithms have been compared. Section 5 describes the calibration of parameters, and section 6 describes the comparison of the algorithm with nonpolarimetric methodologies of rainfall estimation.

2. Measurement systems

a. Meteorological radar

The algorithm has been applied to the C-band polarimetric radar at Monte Settepani in Savona, Italy, which is located in a high topographical environment. This is an operational-switched dual-polarization radar and is currently used by the Meteorological Weather Services in the Italian regions of Piemonte and Liguria and by the Italian Civil Protection Department. The characteristics of the radar and its polarimetric scan strategies are described in Tables 1 and 2.

b. Rain gauge network

Rain gauge data have been acquired by the Liguria and Piemonte regions' real-time networks. There are about 200 stations—each station is provided with a rain gauge—with different sampling times ranging from 5 to 30 min. These stations belong to the Italian Operational Network, which is one of the largest operational networks in the world with more than 1500 rain gauges distributed across Italy.

One of the aims of this work was to understand if the proposed algorithm is able to estimate the rainfall rate where radar can detect data with sufficient reliability. For this reason we decided to eliminate from the comparison all the gauges that are over a certain distance from radar or are located in shielded locations. We chose 100 km as the limit on distance, and we decided not to consider those rain gauges that are located where the first unshielded elevation has an elevation angle larger than 0.3°. The first and second elevations correspond to −0.3° and 0.3°, respectively; it must be taken into consideration that the radar altitude is 1400 m, so a negative elevation is justified. In this way we tried to eliminate the cases in which bad rainfall estimation is mainly due to physical reasons (e.g., shielded locations, bright band, solid precipitation) and not to the proposed algorithm.

In Fig. 1 the location of radar and rain gauges in use are shown together with the visibility map, where every shade of gray represents an elevation. The lighter shade corresponds to the first elevation (−0.3°) and the darker shade to the fifth elevation (2.8°).

c. Dataset

An algorithm for clutter elimination is applied in real time to raw radar data before calculating rainfall (Silvestro et al. 2005). Maps of precipitation are generated on a regular grid, with a spatial resolution of 1 km × 1 km. Rain rate is calculated by considering data from the lowest unshielded elevation, identified by an analysis of visibility based on a digital elevation model. The nearest rain gauge is 1 km, the furthest is about 100 km from the radar, and the mean distance of the rain gauges in use is about 40 km. Because the radar bin has a radial resolution of 0.3 km and the beamwidth is 1°, the resolution cells are 0.3 km × 0.02 km for distances of 1 km and 0.3 km × 1.8 km for distances of 100 km; a typical resolution cell is about 0.3 km × 0.7 km.

The Monte Settepani radar was upgraded to detect ϕ_{DP} in July 2005. Between September 2005 and October 2007, we have collected and analyzed data from nine significant events. We considered events that occurred during the time when the radar worked at its optimum, without any technical problems and without any loss of

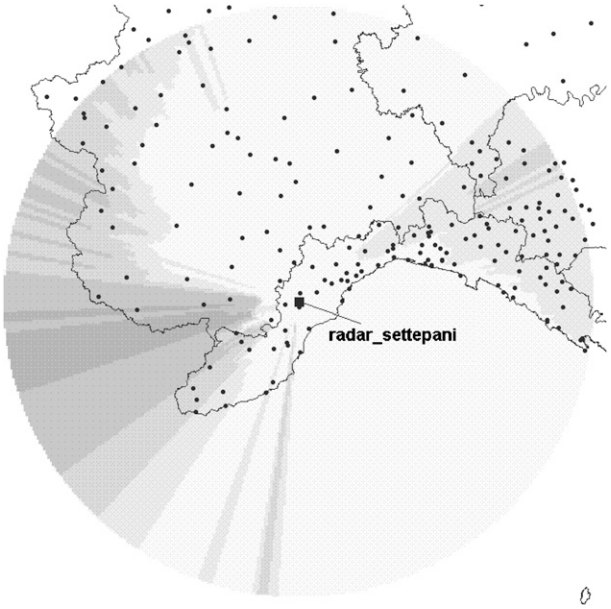

FIG. 1. Location of radar at Monte Settepani. The square is the radar, the circles are the rain gauge used for radar–gauge comparison. The map of visibility is plotted in grayscale: five shades corresponding to the first five elevations. The two clearer gray levels represent the first (−0.3°) and second (0.3°) elevations, respectively.

data. We also applied the algorithm for a continuous period between April and October 2007 but only two relevant events occurred, and we cannot draw any significant conclusion about its routine application.

3. Description of the algorithm

a. Radar intensity multiparameter estimator

Following the Fort Collins flash flood in 1997, Colorado State University developed an algorithm designed to estimate rainfall rate using dual-polarization radar data (Carey and Rutledge 1998; Petersen et al. 1999). More recently modifications have been made, and the algorithm has been applied to a number of events (Cifelli et al. 2003). We adapted this algorithm for real-time application at C-band, with the aim of carrying out comparisons with rain gauge measurements in an operational framework. For this reason we tuned the algorithm thresholds to find the best estimation of precipitation,

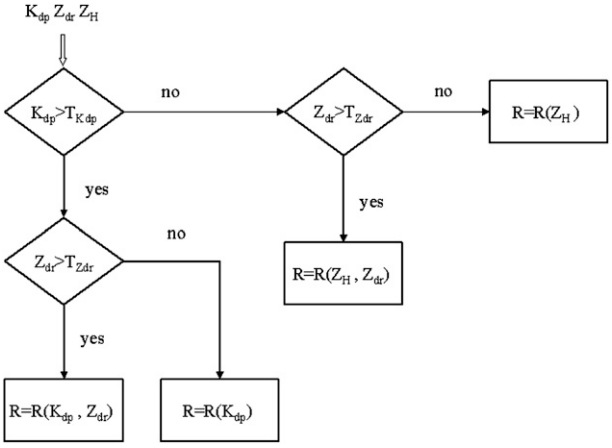

FIG. 2. Flowchart representing the algorithm with Z_H, Z_{DR} and K_{DP} as the input variables, and $T_{K_{DP}}$ and $T_{Z_{DR}}$ as the thresholds on variables. The output is the rain rate calculated with one of the shown formulations.

having as an input the radar measurements specific differential phase (K_{DP}), reflectivity (Z_H), and differential reflectivity (Z_{DR}). An analogous algorithm has been implemented in the software of the Italian National Radar Network. The algorithm consists of a flowchart that combines single tests for deciding which formulation for rain intensity estimation is the most suitable. The aim is to use alternatively the optimal measured variables for calculating the precipitation; in this way we use each moment in the range where its estimates can be consider more reliable, and the rain-rate formulas give physically reliable results. For example, if we have very intense precipitation the Z_H will probably be attenuated, and if we have light rain the differential phase (and so K_{DP}) will be subject to large uncertainty. The proposed algorithm is shown in Fig. 2.

The formulations adopted here have been derived for C-band by Bringi and Chandrasekar (2001). The task of this work was not to find new formulations or a new parameterization for existing formulations but to show the operational benefits of using and combining many polarimetric relationships for rain-rate estimation. The multiparameter, multirelationship algorithm presented here is named rain intensity multiparameter estimator (RIME), and it uses the following relationships for rain-rate estimation:

$$R(K_{DP}, Z_{DRC}) = 39.7K_{DP}^{0.98}10^{0.1(-1.69)Z_{DRC}} \quad (\text{if } K_{DP} > T_{K_{DP}} \text{ and } Z_{DRC} > T_{Z_{DR}}), \tag{1}$$

$$R(Z_{HC}, Z_{DRC}) = 0.0058Z_{HC}^{0.91}10^{0.1(-2.09)Z_{DRC}} \quad (\text{if } K_{DP} \le T_{K_{DP}} \text{ and } Z_{DRC} > T_{Z_{DR}}), \tag{2}$$

$$R(Z_{HC}) = 0.005Z_{HC}^{0.625} \quad (\text{if } K_{DP} \le T_{K_{DP}} \text{ and } Z_{DRC} \le T_{Z_{DR}}), \quad \text{and} \tag{3}$$

$$R(K_{DP}) = 31.4K_{DP}^{0.7} \quad (\text{if } K_{DP} > T_{K_{DP}} \text{ and } Z_{DRC} \le T_{Z_{DR}}). \tag{4}$$

The rain-rate formulation $R(Z_{HC})$ is the well-known Marshall–Palmer formulation (Marshall et al. 1955). In the Z_{HC} and Z_{DRC} notation, the letter C stands for "corrected" and indicates that Z_{HC} and Z_{DRC} are used in the algorithm after they are corrected from path attenuation. The adopted methodology for path attenuation correction is discussed in appendix A and B.

The relationships 1, 2, and 4 are presented in Bringi and Chandrasekar (2001). Their coefficients have been determined by performing nonlinear regressions analysis on tables that report rain rate versus radar variables (rain rate versus Z_H and Z_{DR}). The tables have been constructed generating different gamma drop-size distributions by independently varying the parameters N_w D_0 μ over the following ranges: a) $10^3 \leq N_w \leq 10^5$ mm^{-1} m^{-3}, b) $0.5 \leq D_w \leq 2.5$ mm, and c) $-1 \leq \mu \leq 5$.

Thresholds $T_{K_{DP}}$ and $T_{Z_{DR}}$ represent two free parameters of the algorithm that need calibration. In section 5 the parameters' sensitivity analysis is carried out and discussed.

The trend of differential phase along the beam is very noisy, affected by aliasing and backscatter differential phase problems (Bringi and Chandrasekar 2001), and the last issue becomes even more important because we are working with C-band radar. To reliably estimate K_{DP}, we filtered and corrected ϕ_{DP} with the methodology discussed in appendix A; K_{DP} can be considered reliable only if we are in the presence of a substantial gradient of differential phase.

We added another test before using K_{DP} (Cifelli et al. 2003). By inserting a threshold on Z_{HC}, we avoided those errors in ϕ_{DP} processing that cause a negative influence on rainfall estimation. The threshold was set to 20 dBZ; RIME does not use K_{DP} if the corresponding Z_{HC} is less than this value.

A verification of the physical consistency of K_{DP} estimations has been made; Z_{HC} and K_{DP} data have been plotted on the same diagram (Fig. 3), and the trend is comparable to those reported in Bringi and Chandrasekar (2001, chapter 7.4; their Figs. 7.85a,b) and in Bringi et al. (2001). Clearly data in Fig. 3, coming from an operational system, have a larger dispersion with respect to Bringi and Chandarasekar's (2001) Fig. 7.85b. Furthermore, in some cases K_{DP} estimation is not ideal and may be unrealistic. What is important is that the data that is being generated by the algorithm is physically consistent.

b. Z–R relationships

Another task was to understand if RIME works better than the classical Z–R relationships used in operational frameworks and to discern if polarimetric variables can provide an improvement in rainfall estimation, without any correction or combining techniques with gauge data. We chose three Z–R formulations used in operative frameworks, and we produced rainfall estimations for the defined test cases. The formulations for the test cases are as follows:

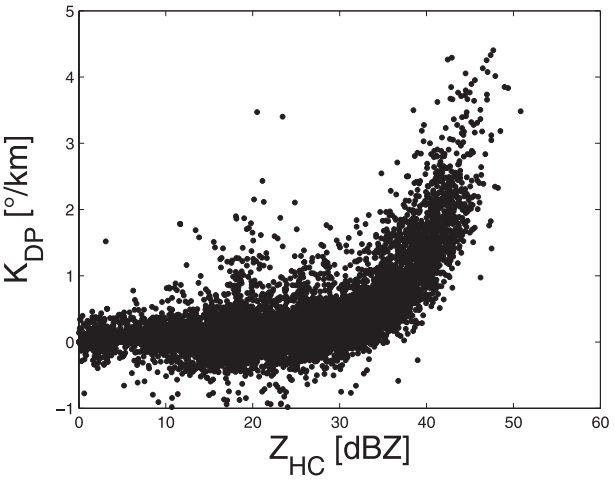

FIG. 3. Graph representing Z_{HC} against K_{DP} derived from the operational scans of radar at Monte Settepani.

$$Z_H = 200R^{1.6} \quad \text{(Marshall et al. 1955)} \tag{5}$$

$$Z_H = 250R^{1.5} \quad \text{(Huggel et al. 1996)} \tag{6}$$

$$Z_H = 300R^{1.4} \quad \text{(Fulton etal. 1998).} \tag{7}$$

These are commonly used in operational radar networks; for example, the Eq. (7) is used in WSR-88D–Nexrad. A great number of Z–R relationships exist, and various works about the parameters' calibration have been made. Different formulas should be used for different types of precipitation, climatic conditions, topographic context, and consequently, the application in real-time situations makes it necessary to simplify the approach and often a single Z–R relationship is used. Recently, more complicated methodologies based on neural networks have been implemented (Liu et al. 2001). They only use the reflectivity factor as a radar variable, but their application is more complex and they are still not used in operational frameworks. Furthermore, they need external information, such as rain gauge precipitation, as input data.

Because in operational frameworks a system of real-time bias correction by rain gauge measurement is often implemented, we also compared the results of RIME with those obtained by applying bias adjustment to the Z–R relationship rainfall estimation. This issue is discussed in section 6.

4. Radar and rain-gauge data comparison

a. Issues about radar–rain gauge comparison

After applying the algorithm to the events, we have to decide how to find out if and how the algorithm works. A way that is followed by several authors (e.g., Ryzhkov et al. 2005) is to compare radar rainfall estimations with rainfall data from rain gauges. This appears to be a simple task, but the different nature and characteristics of the two methods of measurement create many problems (Zawadzki 1975).

Radar data provides a nondirect estimation of the precipitation at a certain altitude from the surface. These data represent a mean value on a certain volume, the dimension of which increases with the distance from radar. Radar measurements are representative of the instantaneous state of the atmosphere. We do not have information about what happens in the time between successive scans. Rain intensity is usually considered constant, but we know that perturbations move and rain intensity changes.

The comparison must be carried out with the measurements on the land surface made by rain gauges, which are continuous and in a particular location.

To account for these problems, we followed the approach presented in the next subsection.

b. Radar–rain gauge comparison methodology

Radar rainfall estimation is provided on a regular grid measuring 1 km $\times$ 1 km. As a test variable, we considered the total rainfall accumulation over the entire precipitation event to reduce the affect of rain variability in space and time. We considered the rainfall estimated by radar above nine grid cells: the one that contains the rain gauge and the eight adjacent cells. The value chosen as the radar measurement for the comparison is the value that minimizes the absolute difference with the gauge measurement (Fig. 4).

Why have we chosen this method instead of others? We could have used the mean radar precipitation of the nine grid cells or the radar precipitation in the cell that contains the gauge. But our aim was to discover if radar is able to detect the rain measured by the gauge—at least in proximity to it, trying to overcome the problems caused by the two instruments not measuring the same variable. For example, we can think about localized peaks of precipitation, characterized by high spatial–temporal variability, where the most intense rain could occur when the radar is not measuring it. This could lead to under- or overestimation of total rainfall. The uncertainty of radar–rain gauge comparison increases when the spatial–temporal scales of the rainfall events are small. By choosing nine grid cells centered on the one over the rain gauge, we can attempt to reduce this uncertainty.

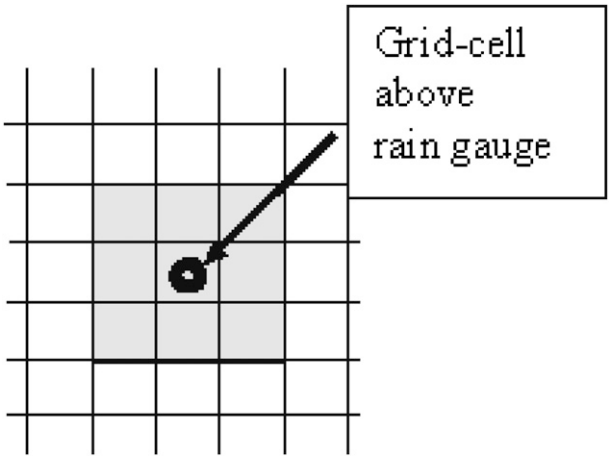

FIG. 4. Scheme of grid cells used for comparison. The nine cells considered are shown in light gray, and the central grid cell shown by the black dot above rain gauge.

It could be more physically based to introduce an independent information like advection velocity, which is determined by radar data; however, this adds new problems: how to evaluate this information and how to overcome problems caused by its poor and unreliable estimation. The pixel chosen for each technique of rainfall estimation can be different for the same rain gauge and time interval; however, this does not ''penalize'' any of them—in fact, for each algorithm the best estimation is chosen.

Another possible solution is represented by the analysis of areal means interpolating rain gauge measurements (Ryzhkov et al. 2005). This approach has two problems, particularly for operational radar and gauge networks: (i) the choice of the interpolation method, and (ii) the inhomogeneity of gauge distribution on land surface.

We consider rain measured by gauge as ''real rain,'' ignoring that it could be affected by systematic and random errors (Habib et al. 2001), a bad gauge localization, malfunctioning, and problems of gauge correction algorithm for intense precipitation.

5. Calibration of thresholds

The first interesting issue to investigate is the choice of the thresholds $T_{K_{DP}}$ and $T_{Z_{DR}}$, which are the two main parameters of the algorithm. As a matter of fact, the parameters of the Eqs. (1)–(4) represent other parameters of the algorithm, but we decided to keep them fixed. We did this to consider a hypothetical operational use of the algorithm and to reduce the degrees of freedom of the system. The sensitivity analysis of these parameters is outside of the aims of this work but could be the subject

TABLE 3. Test events characteristics. The average accumulated rainfall is calculated as the mean of the accumulated rainfall over the entire event for every rain gauge. Also included is the maximum accumulated rainfall measured by a rain gauge and the number of rain gauges that measured a precipitation greater than 2 mm over the event.

		Cumulated rainfall		
Date	Duration (h)	Mean (mm)	Max (mm)	No. of gauges
27 Sep 2005	5	12	134	102
25 Oct 2005	6	16	224	28
2 Dec 2005	36	68	194	75
6 Jul 2006	3	30	136	60
16 Aug 2006	8	50	337	40
14 Sep 2006	24	138	290	106
7 Dec 2006	36	71	190	82
17 Sep 2007	3	20	117	47
1 Jun 2007	6	27	228	120

of future work. Then we analyzed the behavior of the algorithm by considering all the possible combinations of the two sets of thresholds:

$$T_{K_{\mathrm{DP}}} = 0.2,\ 0.5,\ 1.0^{\circ}\ \mathrm{km}^{-1}, \quad \text{and}$$

$$T_{Z_{\mathrm{DR}}} = 0.5,\ 1.0,\ 1.5\ \mathrm{dB}.$$

We generated the fields of precipitation corresponding to each one of the nine thresholds combinations, and we carried out a comparison between rainfall estimated by radar and measured by gauges using bias $= \langle \Delta \rangle$ and SD $= \langle\, |\Delta - \mathrm{bias}|^2 \,\rangle^{0.5}$ as error estimators (SD is standard deviation); $\Delta = P_r - P_g$ is the difference between radar and gauge rain totals from the beginning to the end of an event for any given radar–gauge pair, and angle brackets represent averaging over all pairs.

All the events considered in this work are listed in Table 3. We applied the calibration to four events chosen from the case studies, and in the following brief description we report their main characteristics.

The event on 14 September 2006 is a typical case of a Mediterranean autumnal storm. It lasted about 24 h, with accumulated rainfalls of about 200 mm and peaks of 40–50 mm h^{-1}.

The event that occurred on 16 August 2006 was very intense, with hourly peaks of 80–90 mm h^{-1}. This is a particular case because it was persistent (the duration was about 8–9 h) and not typical of a summer thunderstorm.

The event on 2 and 3 December 2005 had the characteristics of stratiform precipitation with high persistence (about 36 h), few peaks of intensity over 30 mm h^{-1}, and bright band at low altitude. This caused some problems of overestimation in those cases in which the algorithm of detection and correction of raw data did not manage to perform an efficient reconstruction of data.

The event on 7 and 8 December 2006 had similar characteristics to the previous: precipitation with high persistence (about 24 h) and few peaks of intensity over 30 mm h^{-1}. For this event, the bright band was at a higher altitude.

To show the results of calibration in a synthetic way, we made two plots for each event: one with the trend of bias and one with the trend of standard deviation. On the x axis we put $T_{Z_{\mathrm{DR}}}$ and on the y axis the error estimators (bias and SD), and we plotted a graph for each $T_{K_{\mathrm{DP}}}$. In this way we are able to evaluate the sensitivity of RIME to changes of the two threshold parameters.

The results are shown in Fig. 5. It is evident that for all of the four test cases, the sensitivity to the value of the threshold $T_{Z_{\mathrm{DR}}}$ is weak and without any substantial variation of bias and SD. The threshold $T_{K_{\mathrm{DP}}}$ can, on the other hand, influence the performance of the algorithm with absolute variations on bias and SD to the order of $10 \div 30$ mm.

For the events on 14 September 2006 and 7 and 8 December 2006, the lower value of $T_{K_{\mathrm{DP}}}$ ($0.2°\ \mathrm{km}^{-1}$) yields the best results; the trend is that the absolute values of bias and SD increase if $T_{K_{\mathrm{DP}}}$ increases.

In the case of the event on 16 August 2006, there is not a significant difference in performance for different $T_{K_{\mathrm{DP}}}$ values because the event was very intense. As a result, all the K_{DP} values were larger than the maximum value of $T_{K_{\mathrm{DP}}}$, so the number of times the branches of the algorithm for $K_{\mathrm{DP}} > T_{K_{\mathrm{DP}}}$ have been used is quite independent from the values of $T_{K_{\mathrm{DP}}}$ chosen for the calibration.

The case of the event on 2 and 3 December 2005 goes in countertrend, in which the absolute values of Bias and SD increase when $T_{K_{\mathrm{DP}}}$ decreases; this is probably due to the problems of bright band and data correction previously described.

Figures 6 and 7 show the scatterplots of rainfall measured by gauge network (x axis) and rainfall estimated by radar with RIME (y axis) for the events on 14 September 2006 and 7 and 8 December 2006. The results for a fixed value of $T_{Z_{\mathrm{DR}}}$ (1 dB) and for the different values of $T_{K_{\mathrm{DP}}}$ are shown.

The analysis of the results of the calibration procedure lead us to choose the following as the values of the two thresholds:

$$T_{K_{\mathrm{DP}}} = 0.2^{\circ}\ \mathrm{km}^{-1}, \quad \text{and}$$

$$T_{Z_{\mathrm{DR}}} = 1.0\,\mathrm{dB}.$$

These values are concordant with what can be deduced from the work of Cifelli et al. (2003) and from the analysis of polarimetric variables ranges in liquid precipitation carried out by Straka et al. (2000). The $T_{Z_{\mathrm{DR}}}$ does not seem to dramatically influence the performances of

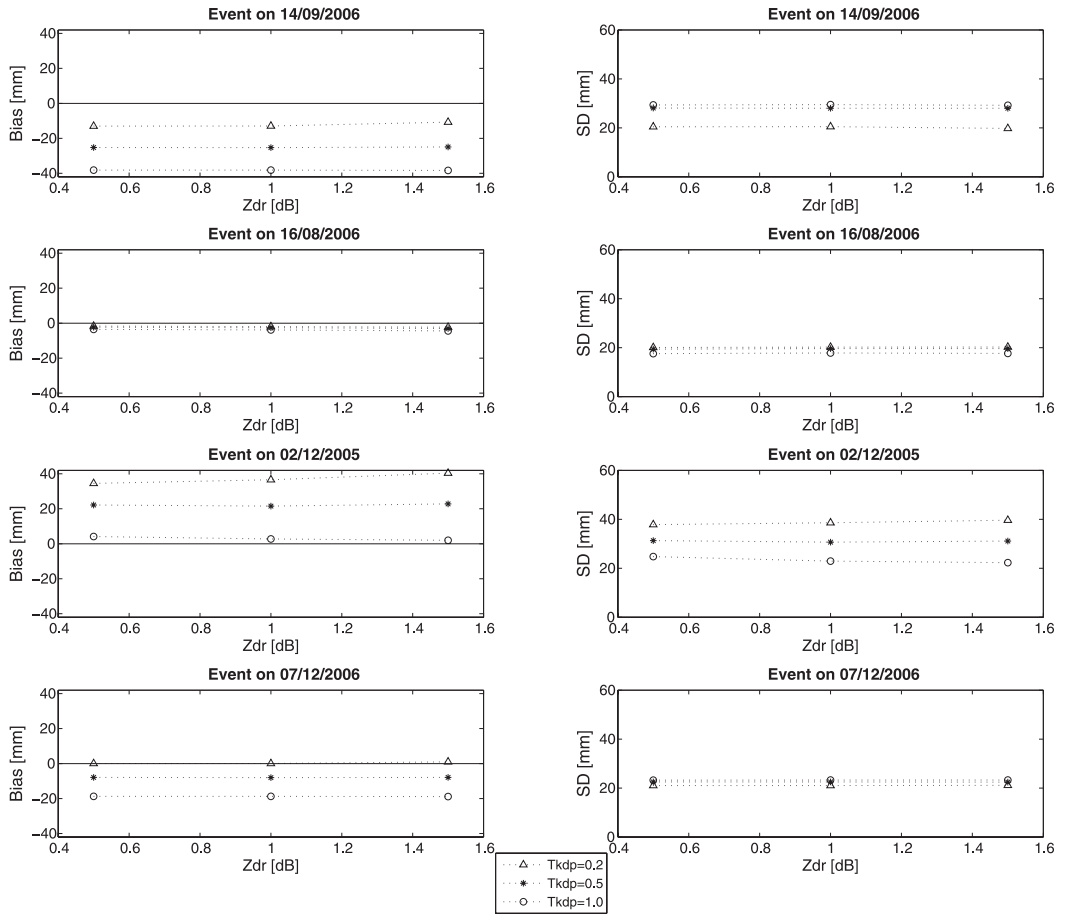

FIG. 5. Thresholds calibration results. On the x axis are the values of $T_{Z_{DR}}$ and on the y axis are the error estimators bias and SD. A graph was plotted for each value of $T_{K_{DP}}$. Two events for warm season and two for cold season were chosen for calibration.

RIME, and perhaps it could be fixed to a lower value for a better estimation of lighter rain. We have decided to use Z_{DR} only in case of quite large drops, considering that the largest values (> 1 dB) of this moment as more reliable and not affected by sampling problems.

Initially, on the basis of our experience and sensibility, we did not consider it reasonable to use K_{DP} values below $(0.4/0.5)^\circ$ km^{-1} for precipitation estimation; however, a lower value of $T_{K_{DP}}$ (0.1° km^{-1}) leads to better results.

6. Application and results

After the thresholds were set, RIME was applied to the events listed in Table 3. The algorithm has been continuously applied for the period April–October 2007. The events selected from this period are those with a larger volume of rainfall and higher intensities, which are the criteria used for the complete capabilities of RIME. All the other rainfall events that occurred during the continuous application were very weak and do not allow for a proper comparison between the algorithms. For a more exhaustive and detailed analysis, it would be necessary to consider a longer period of time and include significant events in the cold season.

The comparison between rainfall estimated by radar and rainfall measured by gauges has been carried out in terms of scatterplot, error estimators [bias, SD, root-mean-square error (RMSE), and mean logged radar-to-gauge ratio (MLR)], and the accumulated contribution to total rainfall, as in German et al. (2004).

To evaluate the quality of different methodologies, we used the following error estimators: bias and standard deviation (refer to section 5), RMSE $= \langle|\Delta|^2\rangle^{0.5}$, and MLR $= \langle\log(P_r/P_g)\rangle$ (Meischner 2004); $\Delta = P_r - P_g$ is the difference between radar and gauge rain totals from the beginning to the end of an event for any given radar–gauge pair, and angle brackets represent averaging over all pairs. Bias, SD, and RMSE are widely used error estimators, and MLR indicates how much we deviate

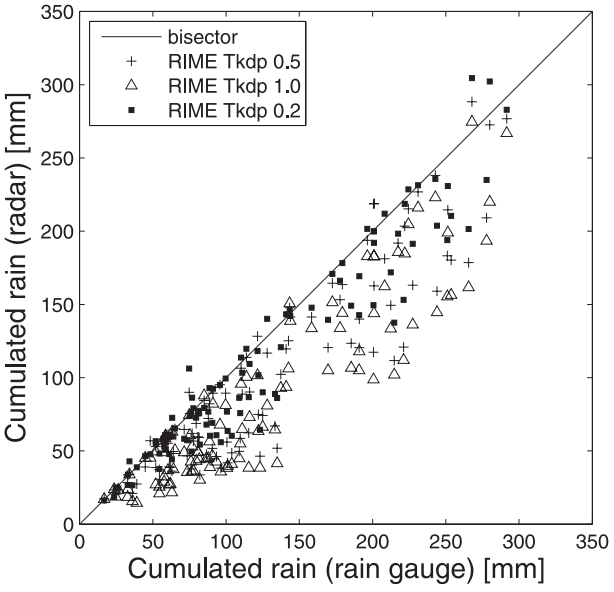

FIG. 6. Scatterplot of radar rainfall and rain gauge rainfall for the event on 14 Sep 2006. Rainfall measured by gauge is on the x axis and rainfall estimated by RIME is on the y axis. Results for $T_{Z_{DR}} = 1$ dB and for the different values of $T_{K_{DP}}$ are shown.

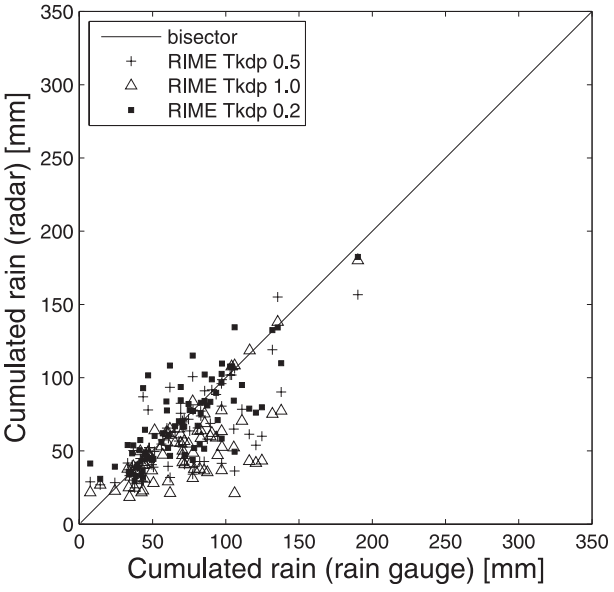

FIG. 7. Same as Fig. 6 but for 7 and 8 Dec 2006, results are for $T_{Z_{DR}} = 1$ dB, and for the different values of $T_{K_{DP}}$.

from the perfect matching radar–gauge pair (MLR = 0) on average. Negative values indicate an underestimation; positive values indicate an overestimation.

The main objective of this work was to evaluate the benefits of using an algorithm based on measurements from full polarimetric Doppler radar in comparison to the use of standard Z–R techniques of rain-rate estimation.

In the first subsection, the comparison with the three Z–R formulations, initially without any kind of correction of Z and R, is described. Then a bias correction was applied to one of the Z–R formulations. In both cases no path attenuation correction of Z_H was applied and, in these cases, Z_H is reported as Z_{HU}.

In the second subsection, the comparison with one of the Z–R formulations used after path attenuation correction of Z_H (indicated as Z_{HC}) is described.

a. RIME and Z–R comparison

In this section we analyze the results obtained from all the case studies, adding the description of rainfall events not reported in the calibration section.

First, we considered the situation of having a nonpolarimetric system and the absence of a reliable real-time rain gauge network. We produced rainfall estimates by using the formulations presented in section 3. Because we wanted to test the performances of the algorithms by using radar measurements alone, we did not apply any kind of bias correction using rain gauge measurements.

Then we considered the situation of having a nonpolarimetric system and the availability of a reliable real-time rain gauge network. We chose one of the formulations presented in section 3 [Eq. (5)], and we produced rainfall estimations; in this case, we applied a bias correction using rain gauge measurements. The methodology is described in Fulton et al. (1998). It is substantially a mean bias correction based on the ratios between precipitation estimated by radar and precipitation measured by gauges; the mean bias is calculated on an hourly scale.

The performances obtained with the two hypotheses were compared with those obtained with RIME.

The values of error estimators are shown in Table 4. The results show a generally better performance of RIME compared to the Z–R relationships in the case of a no-bias correction; when bias correction is applied to the Z–R formulation, the results improve and for some events are similar to those of RIME (e.g., 27 September 2005, 14 September 2006, and 1 June 2007). The use of polarimetric variables leads to having good performances in the quantitative estimation of precipitation without the introduction of external data (e.g., rain gauge data), and this is very useful when a real-time rain gauge network is not available or not reliable. This advantage could be relevant even if a reliable network is present; in fact, avoiding the use of different sources of data can simplify the procedures used to generate rainfall estimation and also to make them more robust and quick.

To clarify the figures, we show only the plots of rainfall estimated by RIME and by Eq. (5) with and without bias correction. We show two events: one considered also for

TABLE 4. Mean bias, SD, RMSE, and MLR of the radar estimates on event rain totals for the five different considered methodologies: RIME, *Z–R* (Z_{HU} – R250, Z_{HU} – R200, Z_{HU} – R300) with uncorrected Z_{HU}, *Z–R* (Z_{HU} – R200bias), with uncorrected Z_{HU}, and mean bias correction. The statistics for every single event are considered.

Date	Algorithm	Bias (mm)	SD (mm)	RMSE (mm)	MLR
27 Sep 2005	RIME	0.19	4.67	4.70	−0.10
	Z_{HU}–R250	−2.37	6.02	6.06	−0.07
	Z_{HU}–R200	−2.25	6.55	6.58	−0.05
	Z_{HU}–R300	−2.13	5.09	5.12	−0.09
	Z_{HU}–R200bias	−0.44	3.35	3.36	−0.04
23 Oct 2005	RIME	−0.64	2.56	2.61	−0.11
	Z_{HU}–R250	−9.44	30.74	31.12	−0.28
	Z_{HU}–R200	−9.49	30.72	31.15	−0.25
	Z_{HU}–R300	−9.17	30.58	31.00	−0.31
	Z_{HU}–R200bias	−6.97	26.56	27.05	−0.08
2 Dec 2005	RIME	36.57	38.60	38.86	0.34
	Z_{HU}–R250	−29.61	38.68	38.93	−0.18
	Z_{HU}–R200	−28.17	38.89	39.14	−0.15
	Z_{HU}–R300	−29.97	38.49	38.74	−0.20
	Z_{HU} –R200bias	23.45	56.14	56.50	−0.22
6 Jul 2006	RIME	4.32	10.09	10.16	0.11
	Z_{HU}–R250	−8.91	16.20	16.30	−0.07
	Z_{HU}–R200	−9.59	16.8	17.04	−0.08
	Z_{HU}–R300	−7.02	15.31	15.45	−0.05
	Z_{HU}–R200bias	−9.45	21.78	21.93	−0.05
16 Aug 2006	RIME	−1.96	20.19	20.28	−0.01
	Z_{HU}–R250	−28.09	56.69	56.98	−0.17
	Z_{HU}–R200	−29.27	58.47	58.76	−0.16
	Z_{HU}–R300	−25.99	53.52	53.79	−0.16
	Z_{HU}–R200bias	−12.35	38.61	38.79	−0.01
14 Sep 2006	RIME	−12.96	20.44	20.55	−0.05
	Z_{HU}–R250	−83.84	47.41	47.67	−0.40
	Z_{HU}–R200	−81.81	47.77	48.0	−0.38
	Z_{HU}–R300	−84.12	46.65	46.91	−0.41
	Z_{HU}–R200bias	−11.72	34.22	34.38	−0.04
7 Dec 2006	RIME	−0.01	21.02	21.13	−0.01
	Z_{HU}–R250	−33.61	26.40	26.58	−0.26
	Z_{HU}–R200	−31.87	26.29	26.45	−0.24
	Z_{HU}–R300	−34.09	26.36	26.53	−0.27
	Z_{HU}–R200bias	−0.55	17.60	17.71	−0.02
1 Jun 2007	RIME	−2.73	8.93	8.97	−0.35
	Z_{HU}–R250	−15.66	20.20	20.32	−0.55
	Z_{HU}–R200	−20.15	24.37	24.53	−0.28
	Z_{HU}–R300	−15.17	18.45	18.56	−0.58
	Z_{HU}–R200bias	−2.31	6.40	6.43	−0.13
17 Sep 2007	RIME	2.11	12.03	12.17	0.1
	Z_{HU}–R250	0.61	12.01	12.15	0.07
	Z_{HU}–R200	0.69	11.93	12.08	0.07
	Z_{HU}–R300	0.77	11.31	11.45	0.07
	Z_{HU}–R200bias	5.7	19.79	20.02	0.09

algorithm thresholds calibration and the other used as an out-of-sample test.

Figure 8 shows the scatterplots of rainfall measured by gauge network (*x* axis) and rainfall estimated by radar (*y* axis) for the event of calibration on 14 September 2006. In general we denote a good agreement between

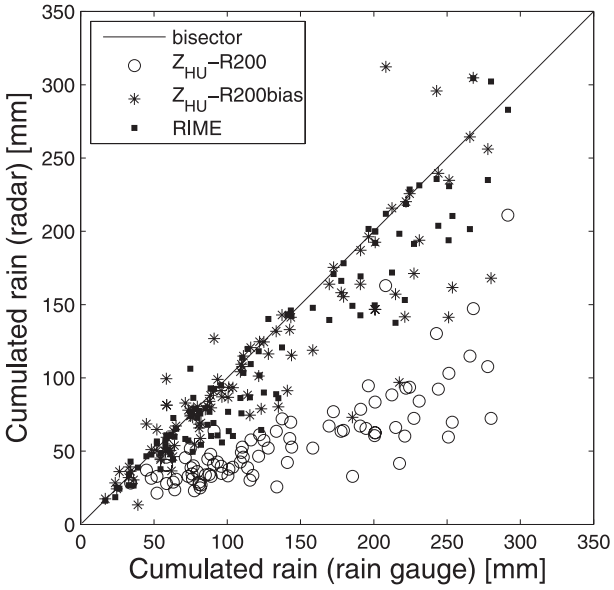

FIG. 8. Same as Fig. 6 but for 14 Sep 2006 and estimated by RIME and by the *Z–R* relationship without bias correction (Z_{HU} − R200) and with bias correction (Z_{HU} − R200bias).

rain gauge observations and RIME that, despite a small underestimation, represents a significant improvement over the standard *Z–R* methodology. The large underestimation of rainfall is probably due to strong attenuation generated by a number of high-reflectivity structures present in the area in which the event is focused. Structures farther from the radar were shielded by other structures closer to the radar. The application of bias correction to the *Z–R* estimation leads to better results, comparable with those obtained by RIME.

Figure 9 shows the contribution to total rainfall (German et al. 2004). The Perfect line represents the perfect estimation. When radar and rain gauge networks observe the same precipitation volume over the entire domain, the maximum value is 1. The difference from this value symbolizes the bias (overestimation or underestimation) for the considered event. The departure from the vertical line explains the differences relative to single gauges. When radar and rain gauge networks measure the same amount of precipitation at each location, the resulting line will coincide with the vertical line of perfect estimation. The diagram shows a considerable improvement of RIME in comparison to the use of the *Z–R* method, with the maximum value of contribution to total rainfall around 0.9 instead of 0.4 and a clear reduction in scatter. The application of bias correction to the *Z–R* estimation leads to results similar to RIME in terms of bias error, but with a slightly larger dispersion (as can be determined from the SD and RMSE values in Table 4).

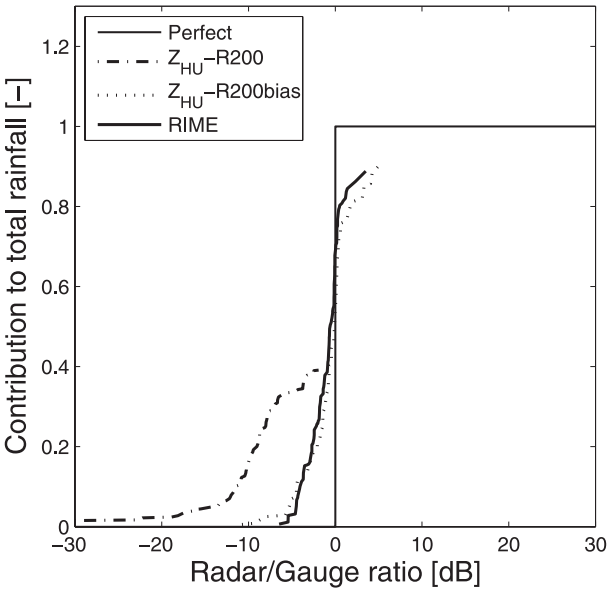

FIG. 9. Accumulated contribution to total rainfall for 14 Sep 2006. The Perfect line represents the perfect estimation. Results for RIME and the Z–R relationship without bias correction (Z_{HU} − R200) and with bias correction (Z_{HU} − R200bias) are plotted.

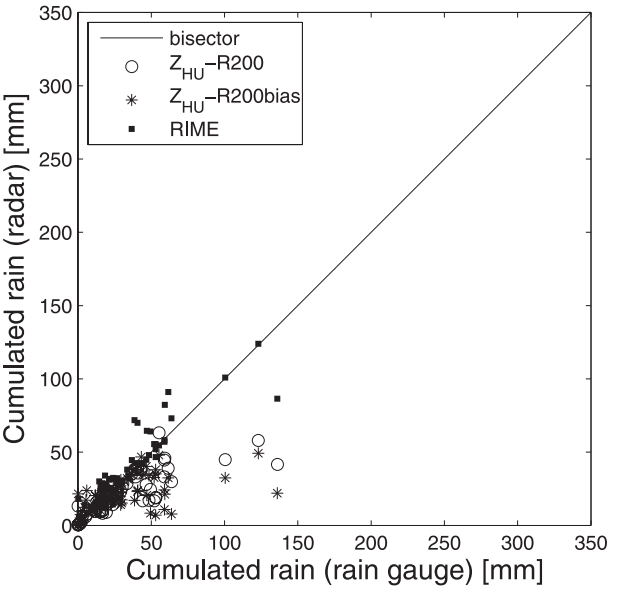

FIG. 10. Same as Fig. 6 but for 6 Jul 2006.

Good results have been obtained for two other calibration events (those on 16 August 2006 and 7 and 8 December 2006) and in particular for the event on 16 August 2006, which shows very low error estimator values and a very high correlation between RIME estimation and gauge measurements with $R^2 = 0.94$. Less satisfactory are the performances in the case of the event on 2 and 3 December 2005 for all the considered methodologies. As already discussed in section 5, the reason for this result was the presence of the bright band at low altitude that caused some problems in liquid precipitation detection.

As in the case not included in the calibration process, we show the plots of the event on 06 July 2006. This event was a classic situation of a summer thunderstorm with a number of showers with maximum durations of 2–3 h and peaks of 30–60 mm h^{-1}.

In this case RIME slightly overestimated the precipitation (maximum contribution to total rainfall = 1.1). The Z–R relationships performed better in comparison to the preceding cases, which also were without bias correction but continued to underestimate the precipitation. The bias correction leads to a generally better result but as can be deduced from the scatterplot, it causes a major underestimation of higher rainfall intensities and total accumulations (Figs. 10 and 11).

The events on 27 September and 23 December 2005 and 17 September 2007 were thunderstorms that lasted for only a few hours and were localized. The results only show large differences when comparing RIME and the Z–R formulations with the event on 23 December 2005. Nevertheless, RIME seems to achieve a better performance for all the other events (Table 4). The good results obtained during the event on 17 September 2007 with the Z–R relationships are due to the not-so-very-strong intensity of the event (less than 25–30 mm h^{-1}), with moderate attenuation along the signal path. In this case the usage of uncorrected

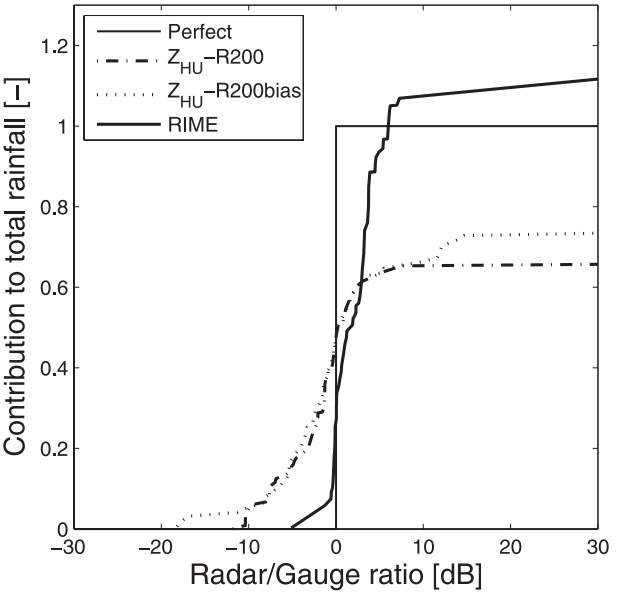

FIG. 11. Same as Fig. 9 but for 6 Jul 2006.

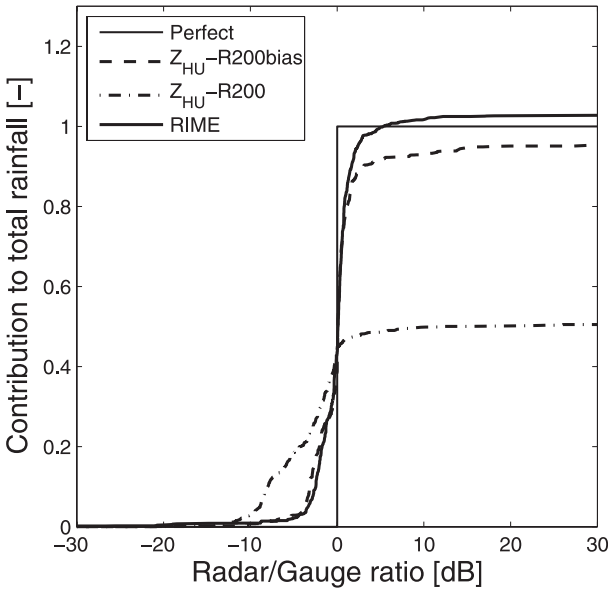

FIG. 12. Accumulated contribution to total rainfall made with all events; Marshall–Palmer formulation is used with (Z_{HU} − R200bias) and without (Z_{HU} − R200) the application of mean bias correction.

reflectivity in the *Z–R* relationships leads to accurate rainfall estimation.

The event on 1 June 2007 was a very intense storm. It occurred between the end of spring and the beginning of summer and lasted for about six hours, with accumulated rainfalls of about 200 mm and peaks of more than 100 mm h^{-1}. RIME and the bias-adjusted *Z–R* method yield similar results, whereas the simple *Z–R* method yields evident underestimation.

The bias correction in various cases leads to similar results for the *Z–R* relationship and RIME, whereas in some other situations, the application of a mean bias adjustment is insufficient to have good results and could lead to counterproductive effects, such as underestimation of intense rain (17 September 2007 and 6 July 2006) or larger SD and RMSE (2 December 2005). RIME seems to be more stable in giving good performances, even though in some events the bias-corrected *Z–R* rainfall estimation produces better bias, SD, and RMSE. By using more sophisticated techniques for bias correction or for the adjustment of radar rainfall estimation by using rain gauge, better results could be obtained with the *Z–R* relationships. However, this leads to methods that are far from the target of simplicity followed in this work and useful for real-time applications.

Figure 12 shows the contribution to total rainfall obtained using data from all the case studies put together. We denote an improvement in quantitative rainfall estimation obtained by RIME in comparison to the use of

TABLE 5. Same as Table 4 but for RIME and *Z–R* relationship with (Z_{HU}–R200bias) and without (Z_{HU} − R200) application of bias adjustment.

Algorithm	Bias (mm)	SD (mm)	RMSE (mm)	MLR
RIME	1.69	22.46	22.48	−0.02
Z_{HU}–R200bias	−2.2	31.45	31.48	−0.01
Z_{HU}–R200	−26.81	42.98	43.02	−0.18

Z–R methods, with the maximum value of contribution to total rainfall of about 1.02 instead of about 0.5 and 0.92 for estimation adjusted and nonadjusted with rain gauges, respectively. The improvement is considerable in the case of nonbias correction with evident bias and scatter reduction, whereas less evident differences are present when we apply a bias correction. Also, the error estimators indicate (Table 5) results that are more similar to RIME, although RIME continues to give better performances in terms of bias and SD.

Figure 13 shows the graphic bar of the percentage of usage of different formulations in RIME. As we thought and in accordance with typical rain intensity distribution (van Dijk et al. 2005), the *Z–R* formula indicated as $R = f(Zh)$, is used much more frequently than other relationships. However, these other relationships seem to have a big impact on rainfall estimation. The relationships that involve polarimetric variables are used much less frequently than the *Z–R* relationship. This is a consequence of the RIME approach, which uses polarimetric variables mainly for high-intensity precipitation. These intensities are statistically less frequent, although they could considerably influence the total volume of a precipitation

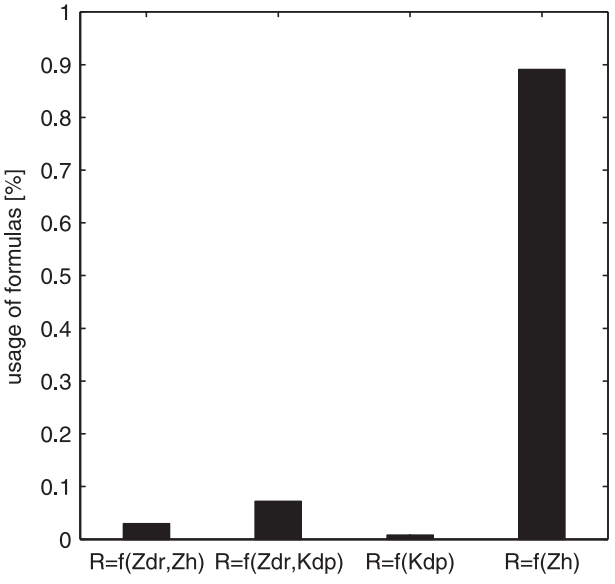

FIG. 13. Bar plot representing the percentage of use of every rain-rate retrieval formulation. Data from all events are considered.

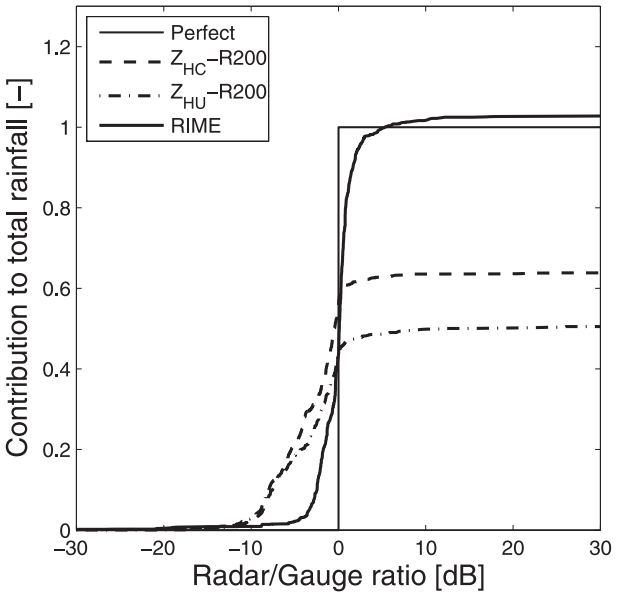

FIG. 14. Accumulated contribution to total rainfall made with all events; Marshall–Palmer formulation is used for both corrected (Z_{HC} − R200) and uncorrected (Z_{HU} − R200) Z_H attenuation.

event and then correspond to the cases in which the values of polarimetric variables are more consistent.

b. *Effect of Z_H attenuation correction on comparison between RIME and Z–R methods*

The graph in Fig. 13 shows that RIME uses the *Z–R* formulation in about 90% of cases. This could suggest that the better performance of RIME in comparison to the *Z–R* formulation mainly results from the use of Z_{HC} corrected for attenuation; therefore, we considered it necessary to investigate this issue further.

We estimated rainfall using the *Z–R* relationship after applying the method of path attenuation correction implemented in RIME and discussed in appendix B, and we compared the results with those obtained with RIME and with the *Z–R* relationship without path attenuation correction. We used Marshall and Palmer's parameters, as in the previous section. In practice it is as if we applied RIME using very high $T_{Z_{DR}}$ and $T_{K_{DP}}$ values.

For simplicity we analyzed the results from all the events shown in Table 3 together.

In Fig. 14 the comparison between RIME and the *Z–R* relationship is illustrated in the case of Z_{HC} (corrected for the attenuation) and Z_{HU} (uncorrected for the attenuation) by using the *Z–R* formulation of the RIME algorithm [see Eq. (3)]. The aim of this last comparison is to show if there are any differences in estimating the surface rainfall amount using RIME, $Z_{HC} - R$, and $Z_{HU} - R$.

TABLE 6. Same as Table 4 but for RIME and *Z–R* relationship with corrected (Z_{HU} – R200) and uncorrected (Z_{HU}–R200) Z_H.

Algorithm	Bias (mm)	SD (mm)	RMSE (mm)	MLR
RIME	1.69	22.46	22.48	−0.02
Z_{HU}–R200	−19.46	31.69	31.71	−0.17
Z_{HU}–R200	−26.81	42.98	43.02	−0.18

The graph shows that there is an improvement between $Z_{HU} - R$ and $Z_{HC} - R$, with a partial correction of bias due to attenuation; however, the use of a full set of polarimetric variables produces a better result in terms of bias correction and minor dispersion around the bisecting line.

We denote a considerable improvement in quantitative rainfall estimation by RIME in comparison to the use of *Z–R* methods, with the maximum value of contribution to total rainfall of about 1.02 instead of about 0.6 for Z_{HC} and an evident scatter reduction.

In Table 6 the values of error estimators are shown; the results indicate a superior performance of RIME in comparison to the *Z–R* relationship in both corrected and uncorrected cases.

7. Conclusions

The aim of this work is the evaluation of the benefits of a methodology that employs polarimetric radar measurements in a real-time framework. A multiparameter algorithm for rainfall estimation using a full set of polarimetric Doppler radar measurements at C-band (RIME) was implemented and applied to some case studies.

The calibration of the two algorithm parameters $T_{K_{DP}}$ and $T_{Z_{DR}}$, discussed in section 5, has shown a weak sensitivity of the algorithm to $T_{Z_{DR}}$, whereas variations of $T_{K_{DP}}$ lead to considerably different results in terms of bias and SD.

Then a comparison was made between rain gauge rainfall measurements and rainfall estimations obtained using RIME.

The performances of RIME were compared with those obtained with two different configurations of a nonpolarimetric radar system:

1) The C-band radar without the availability of real-time reliable rain gauge network. *Z–R* relationships were for rainfall estimation without the application of adjustment techniques by rain gauge data.
2) The C-band radar with the availability of real-time reliable rain gauge network. Mean bias correction technique was applied to radar rainfall estimations.

The results show an improvement deriving from the use of polarimetric variables—in particular, the use of

differential phase ϕ_{DP} leads to a better estimation of rainfall rate in the case of high-intensity precipitation and allows for the correction of Z_H and Z_{DR} measurements. Good agreements between rainfall measured by rain gauges and rainfall estimated by RIME were obtained without any correction or adjustment by rain gauge data.

The introduction of a method for mean bias adjustment to rainfall estimation by the *Z–R* formulation leads to an improvement in the performances that in some cases are comparable to those of RIME; however, in many situations RIME continues to yield better results and sometimes bias correction is counterproductive (event on 6 July 2006).

One more comparison has been carried out to investigate the option of using polarimetric capabilities (i.e., ϕ_{DP}) only to correct Z_H from path attenuation, and then using corrected Z_H in a *Z–R* formulation for rainfall estimation. Results show that the use of an algorithm that can exploit a full set of polarimetric variables leads to better quantitative precipitation estimation.

We adopted an unsophisticated attenuation correction methodology with a fixed parameterization. This is a useful and practical simplification in a real-time framework, but it could lead to a bad attenuation estimation in certain meteorological situations. More sophisticated approaches (Vulpiani et al. 2006) will probably provide a more accurate correction of Z_H and Z_{DR} and could give better rainfall estimations. This, however, would take us away from the target of robustness, simplicity, and calculation rapidity, which is needed for operational applications. The introduction of a better attenuation correction methodology and its effects, could, however, be a matter for future research and analysis.

As a final consideration, we can conclude that the operational use of C-band polarimetric radars seems to lead to a substantial improvement in rainfall estimation compared to traditional radars. Other works (Ryzhkov et al. 2005; Zrnic and Ryzhkov 1996; Bringi and Chandrasekar 2001) showed the benefit of using polarimetry but were mainly carried out with S-band radar systems. The results we obtained show a good applicability in an operational framework, also with reliable rainfall estimations generated through the application of a simple computational chain.

Acknowledgments. This work is supported by the Italian Civil Protection Department and by Regione Liguria. We acknowledge Regione Liguria and Regione Piemonte for putting at our disposal the data of the radar at Monte Settepani (Savona, Italy). We are grateful to the anonymous referees for their helpful reviews and to Mike Whalley for his suggestions in reviewing the quality of the writing.

APPENDIX A

ϕ_{DP} Filtering and K_{DP} Calculation

The processing and filtering of differential phase is absolutely necessary before calculating specific differential phase. Several techniques have been implemented and discussed by different authors, and the one chosen in our application is described by Hubbert and Bringi (1995). It is a low-pass filter based on an iterative finite impulse response filter (FIR). Unlike other methodologies, it has the advantage of identifying the nonzero backscatter differential phase, which is superposed on a monotonic increasing ϕ_{DP} range profile by means of the iteration technique.

The method for K_{DP} calculation is based on a linear regression technique (Bringi and Chandrasekar 2001), which is considered more accurate and robust than the simple finite differences procedure. The calculation of least squares linear fit is done on a varying number of consecutive range samples depending on the reflectivity value measured in the considered bin:

$$Z_H > 45 \text{ dB}Z, \text{ 5 samples}$$

$$30 < Z_H \leq 45 \text{ dB}Z, \text{ 10 samples}$$

$$Z_H \leq 30 \text{ dB}Z, \text{ 15 samples.}$$

The bin radial resolution is 300 m. This leads to the reduction in the effects of statistical measurement errors, which affect K_{DP} more than the conventional radar reflectivity factor; K_{DP} tends to be more uncertain when rain intensity is low. Certainly the application of this method leads to a smoothing of K_{DP} values in light rain; however, in most cases light rain is not estimated using K_{DP} in the presented algorithm. The general philosophy of RIME is respected.

APPENDIX B

Z_H and Z_{DR} Correction

The availability of ϕ_{DP} data enables us to correct the Z_H and Z_{DR} profiles from attenuation caused by the presence of rain along the beam. This phenomenon is particularly evident when we use C- and X-band radar.

Several methodologies of correction based on the use of ϕ_{DP} exist (Bringi et al. 2001; Testud et al. 2000). We chose a very simple method in a perspective of operational real-time application, the linear method, which is based on the belief that the specific attenuation (for C- and X-band radar) has a strong linear dependence on K_{DP}, and the correction of Z_H and Z_{DR} at distance r from radar can be expressed as follows:

$$Z_{\mathrm{HC}} = Z_{\mathrm{HU}} + \alpha[\phi_{\mathrm{DP}}(r) - \phi_{\mathrm{DP}}(0)], \quad \text{and}$$

$$Z_{\mathrm{DRC}} = Z_{\mathrm{DRU}} + \beta[\phi_{\mathrm{DP}}(r) - \phi_{\mathrm{DP}}(0)].$$

In homogenous rain α and β can be estimated by fitting straight lines on pairs of data (Z_H–ϕ_{DP} and Z_{DR}–ϕ_{DP}) obtained from each resolution volume along the path. In our study the two coefficients has been made constant. This hypothesis has been made by other authors (Ryzhkov et al. 2005) for applications and studies. The estimated ranges of variation (Bringi and Chandrasekar 2001) are α [0.04 − 0.15 dBZ $(^\circ)^{-1}$] and β [0.01–0.03 dB $(^\circ)^{-1}$], respectively, and the chosen values are about a mean of these extents:

$$\alpha = 0.08 \text{ dB}Z\ (^\circ)^{-1}, \quad \text{and}$$

$$\beta = 0.015 \text{ dB}\ (^\circ)^{-1}.$$

REFERENCES

Bringi, V. N., and V. Chandrasekar, 2001: *Polarimetric Doppler Weather Radar: Principles and Applications*. Cambridge University Press, 636 pp.

——, T. D. Keenan, and V. Chandrasekar, 2001: Correcting C-band radar reflectivity and differential reflectivity data for rain attenuation: A self-consistent method with constraints. *IEEE Trans. Geosci. Remote Sens.,* **39,** 1906–1915.

Carey, L. D., and S. A. Rutledge, 1998: Electrical and multiparameter radar observations of a severe hailstorm. *J. Geophys. Res.,* **103,** 13 979–14 000.

Cifelli, R., and Coauthors, 2003: Evaluation of an operational polarimetric rainfall algorithm. Preprints, *31st Int. Conf. on Radar Meteorology,* Seattle, WA, Amer. Meteor. Soc., P2B.14. [Available online at http://ams.confex.com/ams/pdfpapers/63992.pdf.]

Fulton, R. A., J. P. Breidenbach, D.-J. Seo, D. A. Miller, and T. O'Bannon, 1998: The WSR-88D rainfall algorithm. *Wea. Forecasting,* **13,** 377–395.

German, U., G. Galli, M. Boscacci, M. Bolliger, and M. Gabella, 2004: Quantitative precipitation estimation in the Alps: Where do we stand? *Proc. Third European Conf. on Radar Meteorology and Hydrology (ERAD)*, Visby, Sweden, Copernicus GmbH, 2–6.

Habib, E., W. Krajewski, and A. Kruger, 2001: Sampling errors of tipping-bucket rain gauge measurements. *J. Hydrol. Eng.,* **6,** 159–166.

Hubbert, J., and V. N. Bringi, 1995: An iterative filtering technique for the analysis of copolar differential phase and dual-frequency radar measurements. *J. Atmos. Oceanic Technol.,* **12,** 643–648.

Huggel, J. S., W. Schmid, and A. Waldvogel, 1996: Raindrop size distributions and radar bright band. *J. Appl. Meteor.,* **35,** 1688–1701.

Jayakrishnan, R., R. Srinivasan, and J. Arnold, 2004: Comparison of raingage and WSR-88D Stage III precipitation data over the Texas-Gulf basin. *J. Hydrol.,* **292,** 135–152.

Liu, H., V. Chandrasekar, and G. Xu, 2001: An adaptive neural network scheme for radar rainfall estimation from WSR-88D observations. *J. Appl. Meteor.,* **40,** 2038–2050.

Marshall, J. S., W. Hitschfeld, and K. L. S. Gunn, 1955: Advances in radar weather. *Advances in Geophysics,* Vol. 2, Academic Press, 1–56.

Meischner, P., 2004: *Weather Radar: Principles and Advanced Applications*. Springer, 337 pp.

Petersen, W., and Coauthors, 1999: Mesoscale and radar observations of the Fort Collins flash flood of 28 July 1997. *Bull. Amer. Meteor. Soc.,* **80,** 191–216.

Ryzhkov, A., and D. Zrnic, 1996: Assessment of rainfall measurement that uses specific differential phase. *J. Appl. Meteor.,* **35,** 2080–2090.

——, S. Giangrande, and T. Schuur, 2005: Rainfall estimation with a polarimetric prototype of WSR-88D. *J. Appl. Meteor.,* **44,** 502–515.

Silvestro, F., N. Rebora, L. Ferraris, M. Morando, P. Alberoni, and A. Fornasiero, 2005: Clutter and rainfall discrimination by means of Doppler-polarimetric measurement and vertical reflectivity profile analysis. *Adv. Geosci.,* **2,** 135–138.

Straka, J., D. Zrnic, and A. Ryzhkov, 2000: Bulk hydrometeor classification using polarimetric data: Synthesis of relations. *J. Appl. Meteor.,* **39,** 1341–1371.

Testud, J., E. L. Bouar, E. Obligis, and M. Ali-Mehenni, 2000: The rain profiling algorithm applied to polarimetric weather radar. *J. Atmos. Oceanic Technol.,* **17,** 332–356.

Van Dijk, A. I. J. M., A. G. C. A. Meesters, J. Schellekens, and L. A. Bruijnzeel, 2005: A two-parameter exponential rainfall depth-intensity distribution applied to runoff and erosion modelling. *J. Hydrol.,* **300,** 155–171.

Vulpiani, G., F. Marzano, V. Chandrasekar, A. Berne, and R. Uijlenhoet, 2006: Rainfall rate retrieval in presence of path attenuation using C-band polarimetric radar. *Nat. Hazards Earth Syst. Sci.,* **6,** 439–450.

Zawadzki, I. I. J., 1975: On radar–raingage comparison. *J. Appl. Meteor.,* **14,** 1430–1436.

Zrnic, D., and A. Ryzhkov, 1996: Advantages of rain measurements using specific differential phase. *J. Atmos. Oceanic Technol.,* **13,** 454–464.